

Hybrid neutron detection optics for gadolinium-acrylic disks in liquid scintillator

Adam S Christensen

A senior thesis submitted to the faculty of  
Brigham Young University  
in partial fulfillment of the requirements for the degree of  
Bachelor of Science

Lawrence Rees, Advisor

Department of Physics and Astronomy  
Brigham Young University

Copyright © 2019 Adam S Christensen

All Rights Reserved

## ABSTRACT

### Hybrid neutron detection optics for gadolinium-acrylic disks in liquid scintillator

Adam S Christensen  
Department of Physics and Astronomy, BYU  
Bachelor of Science

Before low-cost, hybrid neutron detectors can be tested, they must be able to produce strong optical signals. In order to study actual detector conditions, the optics of several detector designs with varying numbers of 2 mm acrylic disks in mineral oil were measured, and the total signal attenuation calculated was calculated. This was accomplished by first determining the amount of signal transmission using laser optics and comparisons with theoretical models of Fresnel Coefficients. The optical efficiency of multiple detector geometries was evaluated. Simulations for an actual detector were then created using Monte Carlo for Neutral Particles (MCNP) which gave information on the photon energies resulting from each neutron interaction. These simulations yielded varying light energies on the order of 0.5 MeVee (electron volt electron equivalent). With an approximate total signal attenuation of 61.2% in both the mineral oil and acrylic disks and an actual attenuation of approximately 62.6%, the resulting optical signal would have energies on the order of 300 keVee. As a result, we were able to conclude that a detector with this geometry would be optically viable.

Keywords: neutron detection, low-cost, optics, hybrid, gadolinium, liquid scintillator

## ACKNOWLEDGMENTS

I would like to express my profound appreciation to Dr. Lawrence Rees for his patient and detailed assistance in my research. His expertise proved invaluable in obtaining data and performing these experiments. I would also like to extend my gratitude to John Ellsworth for his technical and equipment expertise, without which I most likely would have caused some expensive damage. I would also like to acknowledge fellow undergraduate Michael Nelson who was the main creator of the GuiSpec program used in pulse analysis, and finally, extend my gratitude to my wife, Laurel, for her patience with my long research hours and encouragement in persevering to the end.



# Contents

<b>Table of Contents</b>	<b>v</b>
<b>1 Introduction</b>	<b>1</b>
1.1 Introduction to Neutron Detection Research . . . . .	1
1.2 Background . . . . .	2
1.3 Previous Research . . . . .	5
1.4 Current Research . . . . .	6
<b>2 Experimental Methods</b>	<b>9</b>
2.1 Experimental Setup . . . . .	9
2.1.1 Attenuation, Transmission, and Reflection in Acrylic Disks . . . . .	9
2.1.2 Optical Efficiency . . . . .	11
2.1.3 Monte Carlo for Neutral Particles Simulation . . . . .	13
2.1.4 Gadolinium Acrylic Disks . . . . .	14
2.2 Experimental Techniques . . . . .	18
2.2.1 Attenuation and Transmission in Acrylic Disks . . . . .	18
2.2.2 Optical Efficiency . . . . .	20
<b>3 Results and Discussion</b>	<b>21</b>
3.1 Computational Results . . . . .	21
3.2 Optical Data . . . . .	26
3.3 Conclusion . . . . .	29
3.4 Suggestions for Further Work . . . . .	31
<b>Bibliography</b>	<b>33</b>
<b>Index</b>	<b>35</b>



# Chapter 1

## Introduction

In this section, I introduce the factors that motivated my research and my primary goal to characterize the optics for a new geometry of hybrid neutron detectors. These are put into context with a brief discussion of the basic principles involved in neutron detection, specifically with regards to the research that has been performed here at Brigham Young University.

### 1.1 Introduction to Neutron Detection Research

This modern era of technology and energy has seen a meteoric rise in the research of and propagation of nuclear technology. According to the World Nuclear Association, as of January 2019, nuclear energy now accounts for around 11% of the world's electricity and is the second largest source of low-carbon power producing 30% of the total in 2016 [1]. Following the end of World War II, the threat of nuclear attacks from enemy nations or terrorist organizations has been a constant concern of governments worldwide. Whether in a nuclear research facility, nuclear reactor, or issues of national security, it is of paramount importance to be able to efficiently detect nuclear materials, especially those emitting neutron radiation, which pose significant risks to human health and, in the wrong hands, to national security as well.

However, despite the demand, scarcity drives the cost of neutron detector materials higher, inhibiting large-scale production of those detectors. For example, lithium glass scintillator, a material used in neutron detection, commonly costs thousands of dollars per sheet. As a result, interested researchers are currently seeking for ways to reduce the cost of detector production by designing neutron detectors which incorporate available materials while maintaining, and even adding to desired qualities, such as neutron capture efficiency and gamma discrimination.

At Brigham Young University's Nuclear Physics Research Group, we are particularly interested in researching a hybrid class of neutron detector, which reduces overall production cost while maintaining desired effectiveness. However, as hybrid detectors are relatively new, our goal is to properly research and characterize their properties, potential benefits, and limitations so that future researchers or companies could find a viable solution to current problems.

## 1.2 Background

Existing neutron detectors utilize a variety of detection methods in order to capture neutrons, but these methods all have certain properties in common. Since neutrons are neutral particles, unlike electrons or protons, you cannot use electromagnetic fields to observe them. Thus, scientists can only detect and observe neutrons through their secondary interactions with other particles [2]. The most common of these interactions are known as proton recoil and neutron capture.

Proton recoil, as depicted in Fig. 1.1, is a reaction based off of the conservation of momentum. Neutrons, entering a material with a given kinetic energy, collide with protons. As protons and neutrons both have masses of approximately one atomic mass unit, almost all of the neutron's kinetic energy is transferred to the proton, with the exact amount being determined by the angle of incidence. The recoiling nucleus emits ionized radiation, which is then absorbed by the surrounding nuclei. These excited nuclei then emit photons upon de-excitation.

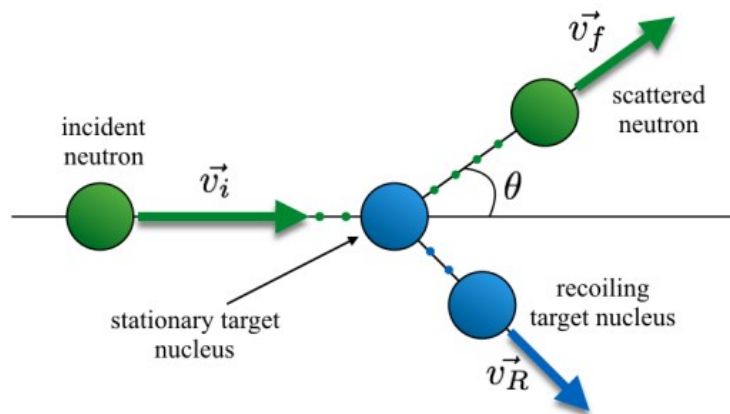


**Figure 1.1** When fission neutrons enter a material with high proton density, collisions with protons produce ionized radiation as shown. Taken from Master's Thesis by Joseph Turko.

Neutron capture, as depicted in Fig 1.2, is another type of neutron-nucleus interaction that occurs with low energy neutrons. Some elements, like gadolinium, have a high probability, or cross section, of capturing low energy neutrons. Upon capturing the neutron, the nucleus becomes unstable due to the increased mass number and then emits gamma radiation in order to restore stability.

We were interested in a type of neutron detector that incorporates scintillating materials. Scintillating material interact with incident radiation and then emit photons when they de-excite to a lower energy level. In order to distinguish nuclear recoil energy from the energy measured by scintillation light, scintillation light is measured in "electron equivalent" units, which will be used throughout this paper. This unit is no different from a normal electron volt in terms of magnitude, but because its source is different, it is convenient to use eVee instead of eV as units for scintillation light. These scintillators also have high concentrations of protons, which efficiently moderate high-energy (i.e. fission) neutrons through momentum conservation.

It is important to note that some scintillator based detectors provide some gamma discrimination ability. Following excitation in stilbene, for example, decay time from gamma radiation lasts around

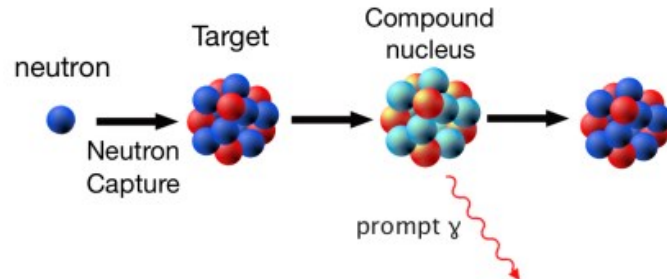


**Figure 1.2** When thermal neutrons are captured by a nearby nucleus, the nucleus emits a gamma particle with an energy specific to the nuclear element. Taken from Doctoral Dissertation by Pretam Kumar Das.

4 ns on average. Faster fission neutrons have decay times more than two times this [2]. Thus, with adequate pulse discrimination capabilities through analysis programs, researchers can, with a measure of uncertainty, distinguish between gammas and neutrons. However, researchers always hope to reduce uncertainty in results, if possible, and thus, we're seeking for other methods.

To combat background radiation, researchers at BYU pioneered dual-pulse scintillators, which combine scintillation materials into a hybrid detector [3]. Fission neutrons enter the detector and are immediately moderated by proton-rich scintillating materials and emit pulses known as proton recoil pulses. Then, once their energy has been moderated, another scintillating material captures the neutron, emitting another pulse, known as the capture pulse. Incident gammas and cosmic radiation produce only single pulses instead of two, allowing discrimination between the two interactions.

Another common issue with neutron detection using scintillators is optical signal strength. Scintillator based detectors use photomultiplier tubes (PMT) in order to measure the incoming photons from proton recoil and neutron capture events. If, due to absorption or repeated reflection, the optical signal strength weakens before measurement at the PMT, it is impossible to distinguish

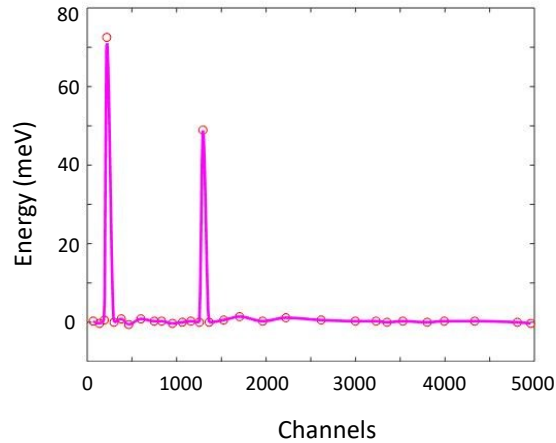


**Figure 1.3** Unlike incident gamma radiation, energetic fission neutrons interact with both types of scintillator producing proton recoil and characteristic capture pulses.

the pulses from background noise.

### 1.3 Previous Research

Researchers at BYU have performed several formal experiments on hybrid neutron detectors. Steven C. Howell, working under Bart Czirr, researched a hybrid lithium gadolinium borate (LGB) crystal and plastic scintillator in an attempt to correctly reproduce the spontaneous emission curve of californium using the LGB detector as a spectrometer [4]. Although they did not complete the data analysis due to complications, researchers already ran many tests on such detectors, which provides some of the unfinished data [5]. Andrew McClellan, working under Lawrence Rees and Bart Czirr, researched a hybrid plastic scintillator lithium glass detector and found 30% neutron detection efficiency with gamma contamination of only 1 in 10,000 events [6]. They also used the predictive Monte Carlo for Neutral Particles (MCNP) code and compared experimental data.

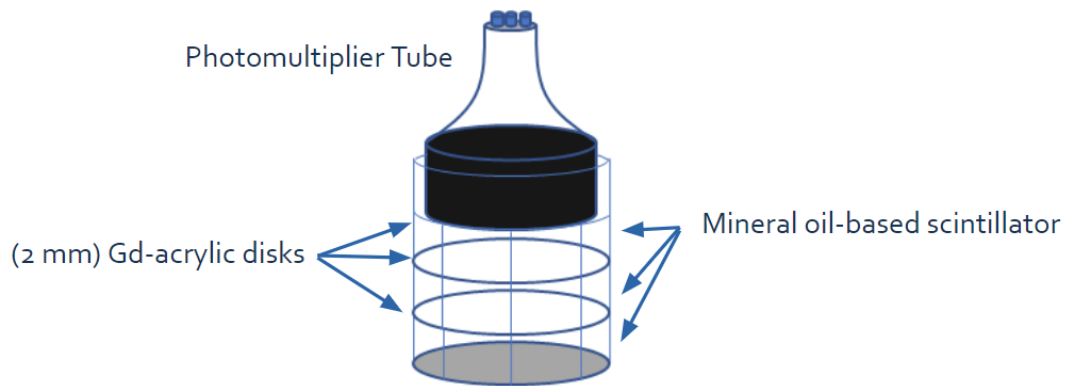


**Figure 1.4** This hybrid detector design incorporates mineral-oil based liquid scintillator, gadolinium infused acrylic disks, and a photomultiplier tube to detect photons emitted from the scintillator. In the schematic, only three disks are shown, but in reality, this could be any number of disks.

## 1.4 Current Research

We're currently researching a new design for hybrid detector with liquid scintillator and gadolinium acrylic, as shown in Fig. 1.4. Before actual construction and detection, we first researched the detectors optical characteristics. The integrity of the optical signal was tested using materials with similar indices of refraction to acrylic and the liquid scintillator EJ-325A. In this particular test, we used one to six acrylic disks in increasing order and standard mineral oil for the liquid scintillator. We used lithium-6 ( ${}^6\text{Li}$ ) glass enriched to 95% at the bottom of the detector to provide photons from capture pulses. However, this optical analysis is meant to provide a base level for optical signal strength. When testing the completed detector, liquid scintillator produces photons throughout the entire volume instead of at the bottom. This reduces the absorption and reflection that occurs throughout the detector.

From optical test data, we homed in on the ideal number of acrylic disks that minimized light absorption and minimized noise from reflection. We then created a model of this design with MCNP,

---

predicting neutron and gamma gamma capture location for neutron energies ranging from thermal to 10 MeV for fission neutrons. As a result of my research, we found that the hybrid detector will produce a minimum of photon energy of 535 keVee (kiloelectron volt electron equivalent) under actual conditions. This value is greater than the standard minimum of 100 keV photons that are routinely detected in existing detectors.

We then proceeded with detector construction by creating acrylic disks with gadolinium isopropoxide particles dispersed throughout each disk. Using these disks, we measured the resulting light attenuation using and compared the data with the predicted model.



# Chapter 2

## Experimental Methods

The goal of this research is to determine if the chosen detector geometry produces optical signals strong enough to be detected and analyzed, a value generally accepted to be 100 keVee (kiloelectron volt electron equivalent). In this chapter, the experimental methods used for each experiment completed during the research are discussed. Sections on the setup for each experiment contain information on the materials and instruments used as well as the desired outcomes. The experimental technique sections then outline the experiments which determine detector optical efficiency and attenuation and transmission in the acrylic disks.

### 2.1 Experimental Setup

#### 2.1.1 Attenuation, Transmission, and Reflection in Acrylic Disks

Because of the crucial role that gadolinium acrylic disks play in moderating high-energy neutrons, we were concerned about the resulting optical consequences of adding these disks into the detector. Specifically, we wanted to know much light will be absorbed and reflected by the acrylic disks and, from that, determine the ideal number of disks to incorporate into the detector. To address

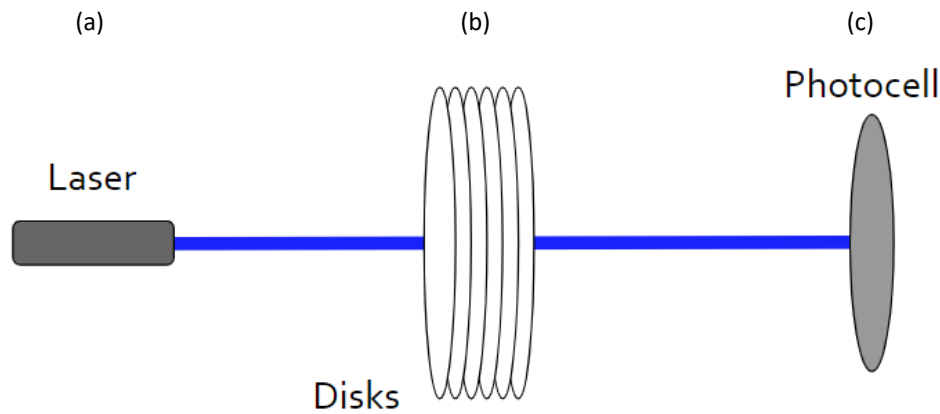


**Figure 2.1** Components used to measure the attenuation of the optical signal at a normal angle to the system. Six 2 mm acrylic disks are depicted although the actual number is varied during the experiment.

this concern in my research, both theoretical and experimental approaches were considered. In order to approximately predict how much light would be transmitted through the detector, the total transmittance of the system, which is defined as the proportion of incident light transmitted, were calculated using the setup shown in Fig 2.1.

In this setup, the number of acrylic disks between the laser and photocell were varied from zero to six. These disks were held flush to one another during the experiment by rubber tipped prongs. For each number of disks, the intensity of the light was measured using an A.W. Sperry SLM-110 photocell for 650 nm, 532 nm, and 405 nm wavelengths of laser light. With the initial intensity and transmitted intensity measured, the transmittance  $T$  can be calculated through a simple proportion of initial intensity and intensity measured through a number of disks.

Once the gadolinium acrylic disks were manufactured, we adopted this same setup, replacing the standard acrylic disks with the new gadolinium acrylic disks.

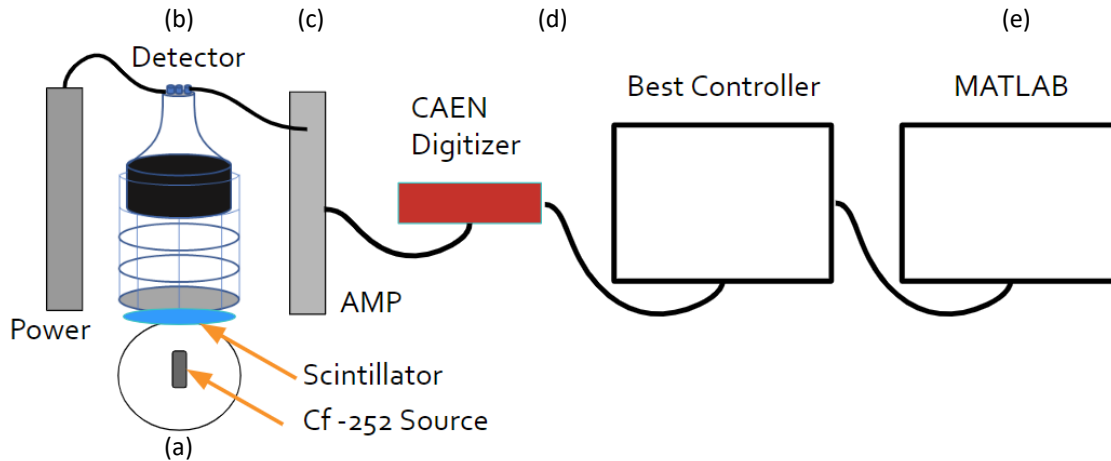


**Figure 2.2** This schematic depicts the five stages with their component parts and their relative location to one another: emission (a), detection (b), amplification (c), digital conversion (d), and analysis (e).

### 2.1.2 Optical Efficiency

To calculate the overall transmittance with acrylic and mineral oil and to qualitatively determine the optical efficiency of the detector, we designed a process using a detector with similar materials and geometry. This process was composed of five stages: the emission stage, the detection stage, amplification stage, digital conversion stage, and the analysis stage.

The schematic for these five stages can be seen in Fig 2.2. Beginning with the detection stage, an aluminized Mylar encased glass cylinder was used as a container for the makeshift detector. Inside the 30 cm height and 7 cm radius cylinder, a 5 cm by 5 cm square piece of lithium-6 glass scintillator emitted photons upon neutron capture or gamma radiation absorption. Six lucite rings with a 11.4 cm diameters were then placed resting on top of the lithium glass sheet as placeholders to keep the acrylic disks separated. The first lucite ring from the bottom had a 5 cm height, and the remainder of the rings had 3 cm heights. The cylinder was then filled up to 20 cm with mineral oil. An Adit photomultiplier tube (PMT) was placed just on top of final lucite ring, making complete contact with the mineral oil. Although the number of disks varied, the number of lucite rings

remained the same since they were also used to hold the PMT in place. To compare the strength of the optical signal for each number of disks, six different configurations of disks were tested. At increasing increments from zero to five disks, 2 mm acrylic disks with 12.8 cm diameter were placed in between each lucite glass ring. The cylinder and PMT components were then placed in a sealed box to prevent light pollution from affecting the measurements.

The radioactive source was a sealed californium-252 placed in the center of a spherical, paraffin wax casing of 8 cm diameter located 10 cm below the bottom of the glass cylinder. This source provided neutrons with a mean energy of about 2 MeV and maximum of about 10 MeV along with gamma radiation.

The PMT used an ORTEC high voltage power supply set to a bias of 1.2 kV. To gather data from the PMT, a 50-ohm coaxial (BNC) cable was attached to the anode output of the PMT, yielding a signal with negative polarity.

In the amplification stage, the coaxial cable was attached from the PMT to an ORTEC amplifier using a female BNC T-adapter with a 100-ohm male terminator on one end to prevent signal reflection and reduce electrical noise. The amplifier's base settings were a coarse gain of x20 amplification and a fine gain of x4.5 amplification, but these settings were adjusted for each trial to prevent signals from exceeding 2 V. Upon output, the polarity was again reversed to positive values and attenuated with a 20 dB BNC attenuator resulting in roughly 1/10 the total signal. The signal can also be taken from the dynode port on the PMT, allowing a bypass of the polarity switching, but the signal is slightly smaller in amplitude. The purpose of the attenuator is to mitigate any high energy signals from gamma absorption that could damage equipment. During the fine-tuning of this system, a Tektronix Digital Phosphor Oscilloscope was used to observe a signal, similar to the one shown in Fig 2.3, from the amplifier output and confirmed that no signals exceeded 2 V in magnitude.

Once the voltage levels were checked, the oscilloscope in the system was replaced with a

CAEN desktop digitizer, which has an maximum peak to peak voltage limit of 6 V. However, from experience, we found that the digitizer operates best around 1.1 V for typical signals. The digitized signals were recorded by a program developed at BYU known as Best Controller. The settings of this sampler were a rising trigger threshold of 40 mV, a DC offset of approximately 45 mV, a minimum width of 4 samples, and a total run time of 15 minutes. These parameters determine which data are identified as pulses by determining a trigger threshold and minimum width. If either of these conditions is not met, the program does not save the information as an event.

Following the digitization and sampling, the resulting data files were then analyzed using a MATLAB program called GuiSpec. This program recorded and plotted each sampled event onto customized plots. These plots could be altered to place different variables on the x and y-axes: Fixed Time Area, Early Area Ratio, Peak Height, Width, Area, and Timing Location. A key feature in GuiSpec allowed me to select a region on those plots, as depicted in Fig 2.5(a), for analysis. Using this feature, I focused on events that occurred at timing consistent with capture events and analyzed the bar graphs showing peak heights, as depicted in Fig 2.5(b). This timing was determined by recognizing that data associated with capture events would most likely occur around 200 ns following the trigger. While not all of these events are capture events, closer analysis of their pulse shapes reveals that the vast majority are indeed capture points.

### **2.1.3 Monte Carlo for Neutral Particles Simulation**

The experiments for optical efficiency and attenuation, though informative, are limited in application. In my experiment for optical efficiency, photons are only produced at the bottom of the glass cylinder by the lithium glass when the actual detector will produce photons throughout the detector. Thus, we wanted to model the optics for a more realistic detector. The Monte Carlo for Neutral Particle (MCNP) simulation, performed by my advisor, models a given neutron detector that has a defined geometry and known materials. The program uses a source defined in terms of emission energy,

which in this case ranged from 0.025 eV thermal neutrons to 5 MeV neutrons. These neutrons are then tracked and, using purely probabilistic calculations, MCNP predicts the ultimate capture location in the detector and the emitted recoil, along with the emitted photon energy in units of eVee (electron volt electron equivalent) from capture events. As photomultiplier tubes routinely measure photon energies of 100 keVee, these simulations, combined with the results from the signal attenuation can predict if the detector will be able to accurately detect proton recoil and capture events.

#### 2.1.4 Gadolinium Acrylic Disks

Following the previous experiments on attenuation and optical efficiency, the next step was to develop a process for creating acrylic disks. Then once this process was mastered, we could introduce gadolinium isopropoxide into the process to create the desired gadolinium acrylic disks.



**Figure 2.3** This image depicts how the stirring stick should be held when pouring acrylic to prevent the introduction of bubbles.

This process consists of five phases: acrylic preparation, removing air bubbles, acrylic casting, pressurizing, and removing from cast. The first phase of acrylic preparation requires a 100 mL PC-400 plastic cup for mixing the acrylic, acrylic plastic casting (we used a one pint bottle from Electron Microscopy Sciences), acrylic hardener (series number: 24210-H also purchased from Electron Microscope Sciences), a silicone O-ring with AS568B number 250, an aluminum ring with inner diameter of 13.5 cm and outer diameter of 14.8 cm, and a wooden stirring stick.

First, we measured out the approximate volume of the cast. We measured the cast volume to be 41 mL, but in order to be certain, poured 50 mL of acrylic into the plastic cup. To minimize air bubbles, we poured the acrylic onto the stirring stick, as shown in Fig. 2.3, and then into the cup.

At this point, hardener should be added to increase the acrylic's rate of curing, and after several trials, we found the ideal amount of hardener to be 12 drops. The hardener was mixed in using the stirring stick for one minute to ensure complete dispersion. The step for air bubbles immediately follows. To remove as many bubbles as possible, we placed the plastic cup containing the acrylic and hardener into an aluminum-foil-lined CentralPneumatic 2-1/2 gallon pressure paint tank outfitted with valves for both vacuum and pressurizing settings shown in Fig. 2.4.



**Figure 2.4** This image depicts a horizontal view of a CentralPneumatic 2-1/2 gallon pressure paint tank used to pressureize the acrylic sample and remove air bubbles.



**Figure 2.5** This image depicts a metal ring, silicone O-ring, and glass plate cast for the acrylic disks.

The lid to the tank was held closed using four fasteners attached to the tank. Keeping the pressurized valve closed, we opened the vacuum valve completely and turned on the Emerson roughing pump. We kept the tank under vacuum for one minute before closing the vacuum valve, turning the roughing pump off, and slowly venting the tank using the appropriately labeled pin.

Once the tank was restored to normal pressure, we removed the acrylic and moved on to the next step by immediately pouring it into the center of the O-ring, metal ring, and glass plate structure shown in Fig. 2.5, again using the stirring stick as a guide for pouring. The metal ring was centered on the glass plate, and the O-ring was then placed completely inside the metal ring so that its outer edge was flush to the inner edge of the metal ring. Once the acrylic filled the entire ring structure, we placed the other glass plate on top of the structure, being careful not to trap air between the acrylic and the glass. Then, we placed four plastic binding clips on each glass edge to hold the plates in place. Once the glass plates were secured, we placed the glass plates inside the tank, returned and secured the lid, and by opening the pressure valve, pressurized the tank to 20 psi. After approximately 40 hours under pressure, we slowly released the pressure using the same pin as with the vacuum. We then removed the glass plates from the tank, and using a thin metal blade, we carefully separated the glass plates from the acrylic disk, finishing the fifth and final step. After this



**Figure 2.6** This image depicts a sealed plastic containment area filled with argon gas for the purpose of storing reactive materials.

process yielded a well-formed disk without bubbles, we repeated the process while adding cupric sulfate into the acrylic before mixing in the hardener to simulate the process using gadolinium isopropoxide. Since cupric sulfate has a bright, blue color and a similar powdery composition, we could qualitatively assess how uniformly it was distributed in the disks and, by extension, if the gadolinium isopropoxide could be similarly distributed. These tests were successful, and the distribution looked uniform throughout the entire disk so we proceeded to add the gadolinium isopropoxide. 0.5 g of gadolinium isopropoxide were purchased from Sigma-Aldrich to be used for the disks. In each disk, we want to include as much gadolinium as possible to maximize the neutron capture cross section. However, as gadolinium isopropoxide is comprised of roughly 47% gadolinium, this means that we have just under 0.25 g of gadolinium to use in the disks. Also, considering that each acrylic disk has a mass of approximately 41 g, using three acrylic disks would yield a 0.2% gadolinium composition. Using two disks would yield a 0.3% gadolinium composition. Although we want to maximize the gadolinium composition, we also need to maximize optical efficiency and minimize light loss from reflection and absorption so all of these factors were taken into consideration and will be presented in Chapter 3.

When repeating this process to fabricate three acrylic disks containing the gadolinium isopropoxide, any remaining gadolinium isopropoxide powder was stored in plastic cups and placed inside an

$\lambda$ (nm)	0 Disks	1 Disk	2 Disks	3 Disks	4 Disks	5 Disks
402	1	0.648	0.428	0.330	0.275	0.185
532	1	0.787	0.584	0.555	0.397	0.365
650	1	0.850	0.617	0.450	0.375	0.317

**Table 2.1** A table of the relative intensities of a given wavelength  $\lambda$  of laser light through  $n$  number of acrylic disks for laser light at 402 nm, 532 nm, and 650 nm

argon-gas-filled containment area, shown in Fig. 2.8, to prevent sample contamination.

## 2.2 Experimental Techniques

### 2.2.1 Attenuation and Transmission in Acrylic Disks

As explained in Section 2.1.1, three wavelengths of laser (e.g. red, green, blue) were shined at normal incidence incident to varying numbers of 2 mm thick acrylic disks. The resulting data were used to calculate the attenuation of the light as it passed through acrylic. To do this, the intensity of light from the photodiode was measured and the relative intensity was calculated using the formula  $I_{\text{rel}} = I_{\text{meas}}(m)/I_{\text{meas}}(0)$ , where  $I_{\text{rel}}$  is the dimensionless relative intensity and  $I_{\text{meas}}$  is the intensity measured at the photodiode for  $m$  number of acrylic disks. The intensity of light measured for each number of disks is listed in Table 2.1. We predicted that the relative intensity would fall off as  $e^{-d*m*a}$ , where  $d$  is the material thickness,  $m$  is number of disks, and  $a$  is the attenuation coefficient of light in a material. The attenuation coefficient is a quantity specific to different materials that can be used to determine how the intensity of light, shined at normal incidence, is reduced given the thickness of material. By using Mathematica to find the linear fit to our data points, the attenuation coefficient was calculated using the slope,  $a$  of the resulting line  $\ln(e^{-d*m*a}) = -d * m * a$ .

To test the accuracy of this assumption, we also calculated the total transmittance of the same

setup using transmission coefficients for multiple parallel interfaces. Transmittance is defined as the proportion of incident light that transmits through an entire material. When multiple parallel interfaces are used, as in this setup, the transmission coefficient is calculated from:

$$t_{\text{tot}} = 1/b_{11}, \quad (2.1)$$

where  $t_{\text{tot}}$  is the transmission coefficient and  $b_{11}$  is the matrix element for the matrix  $B$ , which represents the magnitude of the electric field. This matrix  $B$  is:

$$B = \begin{bmatrix} b_{11} & b_{12} \\ b_{21} & b_{22} \end{bmatrix} = \frac{1}{2 * n_0} \begin{bmatrix} n_0 & 1 \\ n_0 & -1 \end{bmatrix} \prod_{j=1}^N M_j \begin{bmatrix} 1 & 0 \\ n_{N+1} & 0 \end{bmatrix} \quad (2.2)$$

and

$$M_j = \begin{bmatrix} \cos(kd) & -i \sin(kd)/n \\ -i * tn / \sin(kd) & \cos(kd) \end{bmatrix} \quad (2.3)$$

where  $k$  is the wave number for acrylic sheets,  $d$  is the thickness of the acrylic disks,  $n$  is the index of refraction for acrylic, and  $n_0$  is the index of refraction for air. The resulting transmittance  $T$  of the system is:

$$T = |t_{\text{tot}}|^2. \quad (2.4)$$

When the appropriate values for each of the parameters are used Eq. (2.4) yields the results shown in Table 2.2. As the number of disks increases, in general, the overall transmittance decreases. Additionally, there also seems to be a relationship between the wavelength of light and the total transmittance which indicates that increasing wavelength leads to decreased transmittance. However, this is merely an observation from our current data points.

$\lambda$ (nm)	0 Disks	1 Disk	2 Disks	3 Disks	4 Disks	5 Disks
402	1	0.458	0.276	0.279	0.155	0.076
532	1	0.363	0.179	0.184	0.114	0.041
650	1	0.257	0.102	0.105	0.088	0.021

**Table 2.2** A table of the transmittance values for a given wavelength  $\lambda$  of laser light through  $n$  number of acrylic disks

### 2.2.2 Optical Efficiency

In this experiment, the purpose was to find out how the strength of the optical signal decreased as the number of acrylic disks was increased. In an actual detector setting, a greater number of disks means a greater neutron capture efficiency, but comes at the cost of reduced optical signal strength due to reflection loss or other forms of signal attenuation. Through data collection and comparison, I desired to find the number of disks that could be used before the captured signal appeared smaller than the surrounding background noise. To ensure accurate results, the collection time was set to be between 10 to 20 minutes for each run, allowing the data collection system to take over 100,000 capture events. To establish a baseline for the system, the first run had no mineral oil or disks inside the glass cylinder, the second run had mineral oil but no disks included. However, since the actual detector will ultimately have at least one layer of gadolinium-acrylic, the data gathered from these runs were only intended to indicate the change in light absorption that occurred once mineral oil and acrylic disks were added. Following these two initial tests, I proceeded to incrementally increase the number of disks under the two base scenarios, one with mineral oil filling the cylinder and one with only air. The resulting data was then digitized and compiled and analyzed using GuiSpec. These results are presented and discussed further in Chapter 3.

# Chapter 3

## Results and Discussion

In this chapter, I present the results from my experiments measuring the overall attenuation from the model detector, the attenuation from the acrylic disks, and detector simulations using MCNP. From these experiments, I determined that given our chosen detector geometry with three disks of Gd-acrylic, there would be approximately 28% attenuation of the predicted optical signal. This attenuation takes place in both the acrylic and mineral oil, and figures showing the attenuation will be presented. The MCNP simulations provide estimates on scintillation photon energies, which when combined with attenuation rates, show that the minimum photon energies are greater than the 100 keVee standard.

### 3.1 Computational Results

We gathered predominantly two types of data from the Monte Carlo for Neutral Particles (MCNP) simulations: location and light output, which, when analyzed, gives insight into the effectiveness of the detector. We then divided the data into groups based on the energy level of the incident neutrons (e.g. thermal, 0.2 MeV, 0.5 MeV, 2 MeV, 5 MeV, and 10 MeV neutrons)

Specifically, we found that thermal energy neutrons with energy less than 0.025 eV had their first

interaction (i.e. capture event or proton recoil event) within the first 5 cm of mineral-oil-based liquid scintillator, with sparse interactions occurring inside the gadolinium disks. Graphs showing the light output for the recoil and capture events for the predominant elements in the detector indicate that only hydrogen and gadolinium capture events yielded any significant light output. The peak energy from hydrogen capture occurred at 1.9 MeV electron equivalent (MeVee) with decreasing numbers of events occurring as low as the range 0 MeVee to 0.5 MeVee. Gadolinium capture events (see Fig. 3.1(b)) yielded photons with energies ranging from a peak near 0 MeV to a minimum around 6 MeV. Other captures and recoil events yielded little to no net light output.

Our next data sets for 0.1 MeV neutrons produced similar results in some regards, but also differed from thermal neutrons. These neutrons, unlike the thermal neutrons, produced energy from recoil events. In Fig. 3.2(b), Hydrogen recoil events led to light emission peaking at 0.8 MeVee, with a much wider spread of energy emission. In Fig. 3.1(a), Hydrogen capture pulses again resulted in a left-shifted peak at approximately 1.9 MeVee, which was consistent across all incident neutron energies.

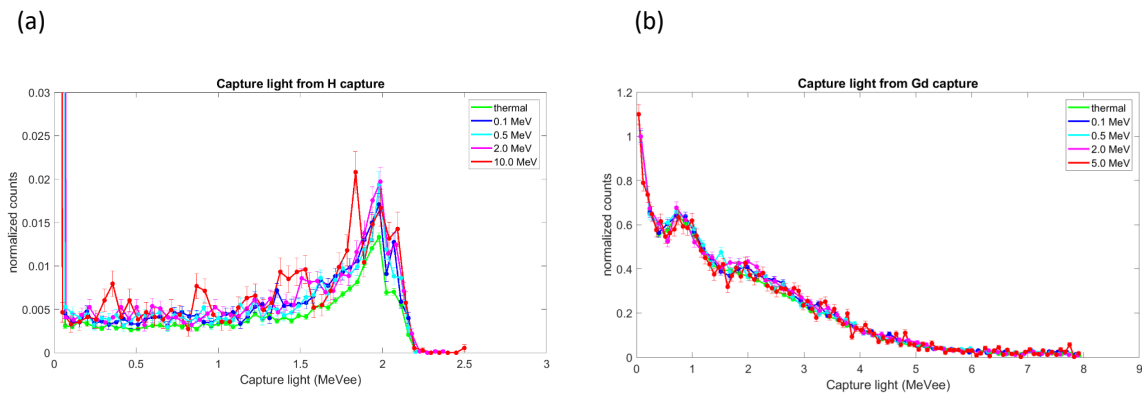


**Figure 3.1** The following plots show (a) photon energies for hydrogen capture events and (b) photon energies for gadolinium capture events. Oxygen capture events are only nonzero for 10 MeV neutrons, which is shown in a later figure.

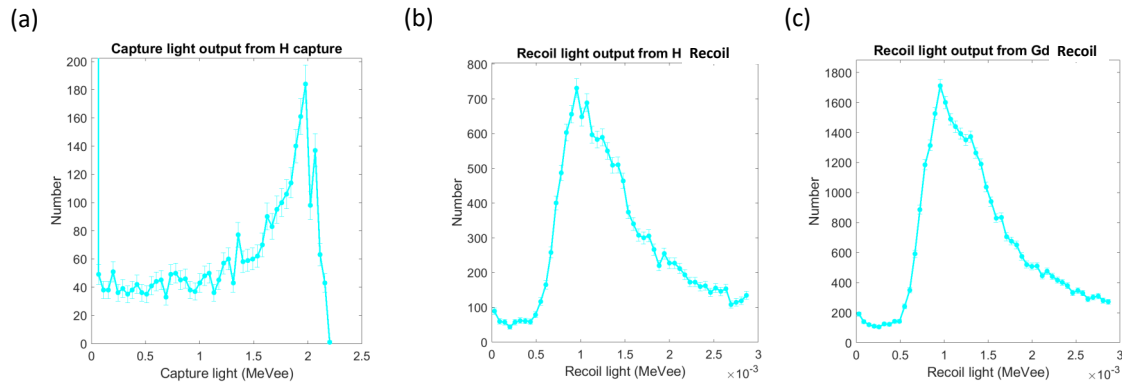


**Figure 3.2** The following plots show (a) photon energies from capture events in hydrogen. No photons are produced from gadolinium and oxygen (b) Photon energy from recoil events for hydrogen and gadolinium in 0.1 MeV neutrons.

For 0.5 MeV, 2 MeV, and 5 MeV neutrons, the capture events yielded very similar photon energies to those in the low-energy neutrons. This is consistent with our understanding of neutron capture events, which produce photons after degrading to lower energy states. The photon energies from proton recoil events in gadolinium and hydrogen produced substantially different results from the lower energy neutrons. For 0.5 MeV neutrons, the photon energies for both gadolinium and hydrogen peak around 0.03 MeVee (See Fig. 3.3(b)) before slowly dropping off towards 0.06 MeV, and these photon energies were around 100 times smaller than the recoil events for 0.1 MeV neutrons. The photons from 2 MeV proton recoil events increased to around 0.4 MeVee (See Fig. 3.4(a) and Fig. 3.4(b)). For 5 MeV incident neutrons, both gadolinium and hydrogen showed photon energies peaking sharply around 1.5 MeVee (See Figs. 3.5(b) and (c)). Finally, some new interactions appeared when looking at the 10 MeV incident neutrons. Unlike the previous cases, neutron capture in oxygen led to photons of significant energies, specifically with peaks just below 1 MeVee and another peak near 2.5 MeVee. The standard proton recoil interactions also showed significant changes, shown in Figs. 3.6(a)-(d). The peaks for proton recoil interactions in

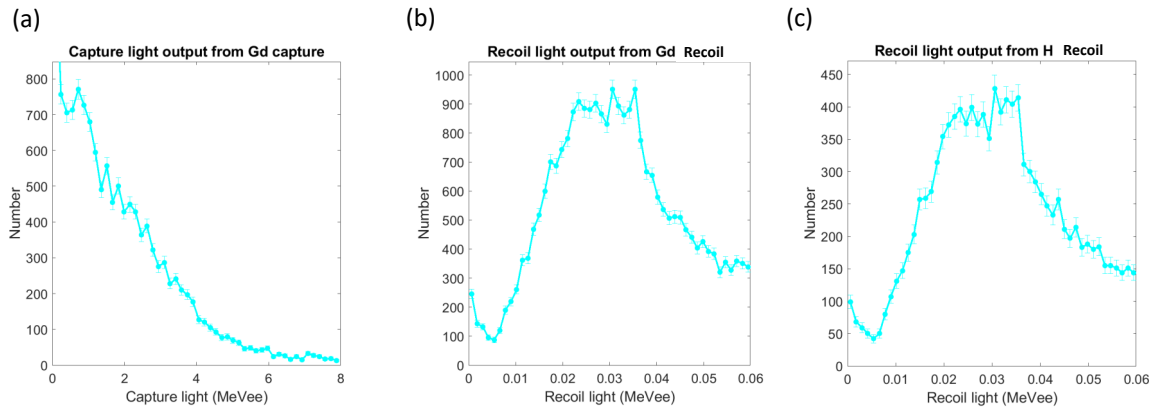


**Figure 3.3** The following plots show (a) capture events for gadolinium. (b) Recoil events for hydrogen and gadolinium for 0.5 MeV neutrons.

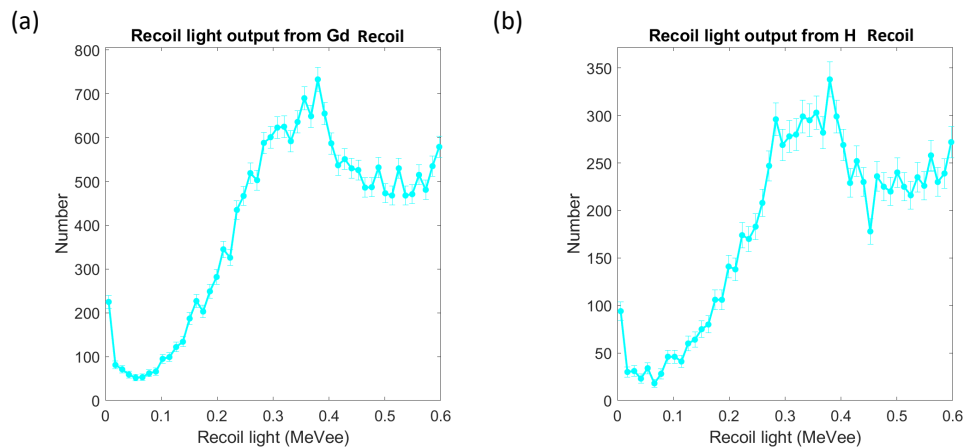


**Figure 3.4** The following plots show (a) capture events for hydrogen, gadolinium, and oxygen. (b) Recoil events for hydrogen and gadolinium for 2 MeV neutrons.

hydrogen and gadolinium shifted to just below 4 MeVee, an increase by more than a factor of two. Surprisingly, some photons were shown from oxygen recoil reactions, but as shown in Fig. 3.6(d), these interactions were very few in number and had comparatively large uncertainties, indicating that these interactions are improbable and unreliable.

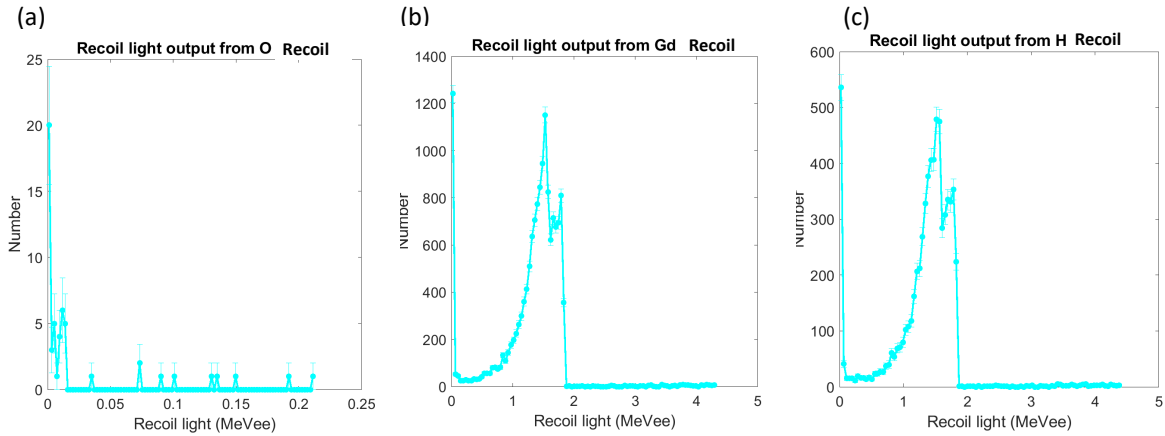


**Figure 3.5** The following plots show (a) capture events for hydrogen, gadolinium, and oxygen. (b) Recoil events for hydrogen and gadolinium for 5 MeV neutrons.

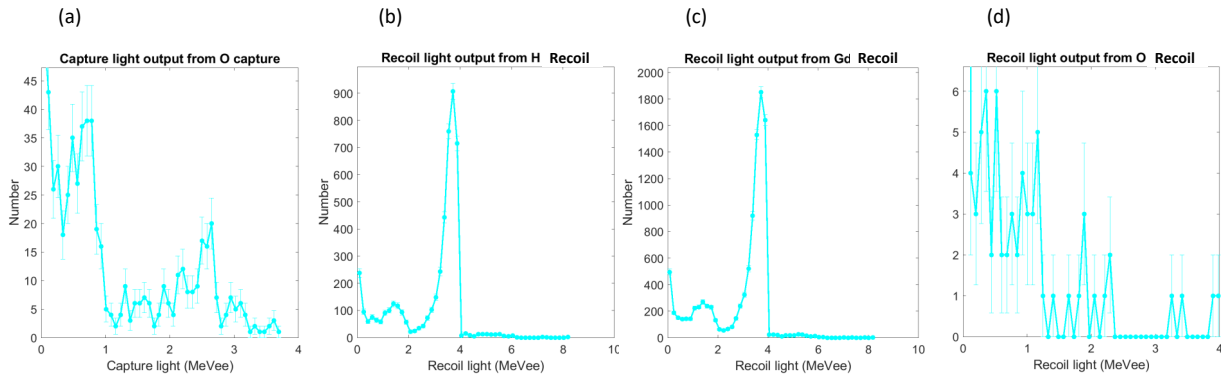


**Figure 3.6** The following plots show (a) capture events for hydrogen, gadolinium, and oxygen. (b) Recoil events for hydrogen and gadolinium for 10 MeV neutrons.

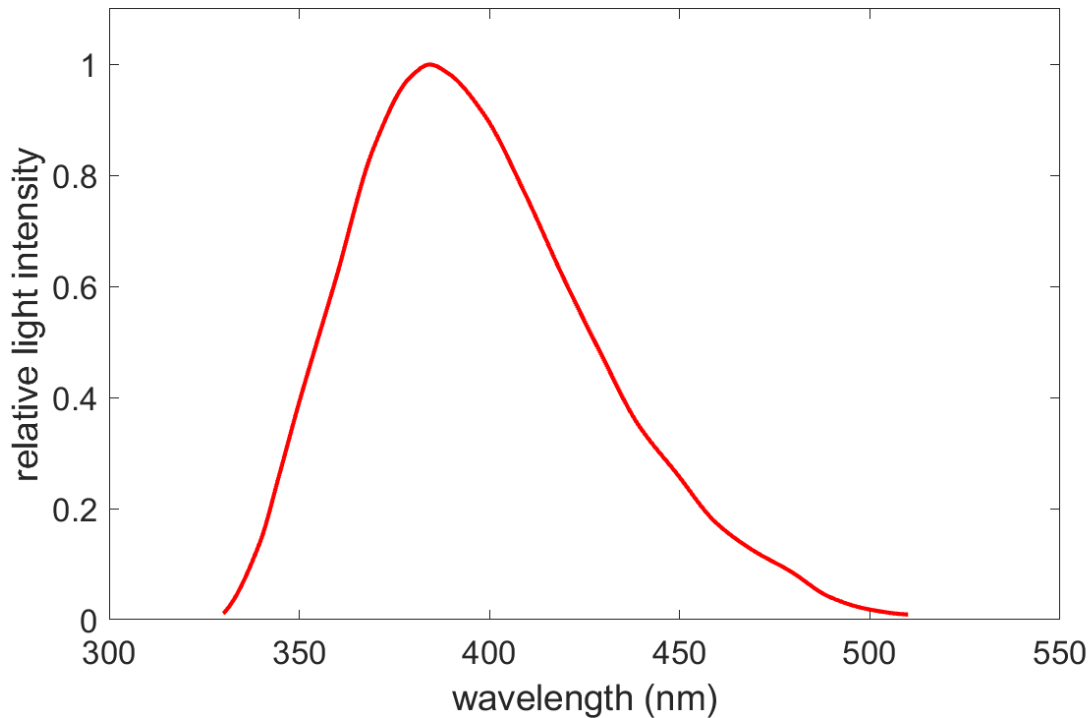


**Figure 3.7** Photon-emission spectrum for lithium-6 glass scintillator

## 3.2 Optical Data

We needed to know the photon wavelength proportionally emitted from our lithium-6 scintillator in order to analyze the detector's absorption. Fig. 3.7 plots the lithium-6 glass' photon emission intensity with respect to wavelength. The photon intensity peaks at just below 400 nm, specifically at 395 nm. As a result, a significant amount of the light emitted will be absorbed by the acrylic inside the detector.

After gathering measurement data for our experimental setup, we noticed that the strength of the optical pulses decreased significantly as we increased the number of 2 mm thick acrylic disks inside the mineral oil. Fig. 3.8 plots the relative light intensity of blue, green, and red lasers as a function of the number of disks. The relative intensity falls off at approximately  $-a * x$  for this plot

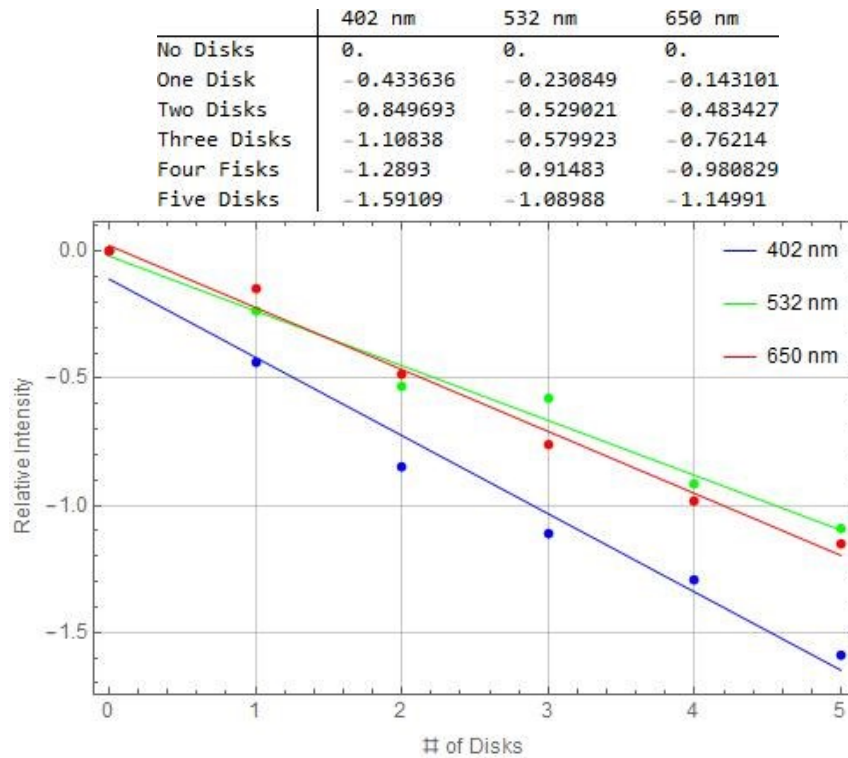


**Figure 3.8** Data points and corresponding linear fit to the natural log of the relative intensity of blue, green, and red wavelengths through 2 mm acrylic disks

**Table 3.1** A list of the calculated attenuation coefficients for the given wavelength  $\lambda$  in 2 mm acrylic disks

$\lambda$ (nm)	Attenuation Coefficient
402	0.33761
532	0.23762
650	0.22068

of the natural log of the data points, where  $x$  refers to the number of acrylic disks and  $a$  refers to a coefficient of attenuation. This confirms what we predicted with our previous plots for lithium-6 glass emissions.

My advisor noted that the attenuation data typically falls off as  $e^{-a*x}$  where  $a$  is determined

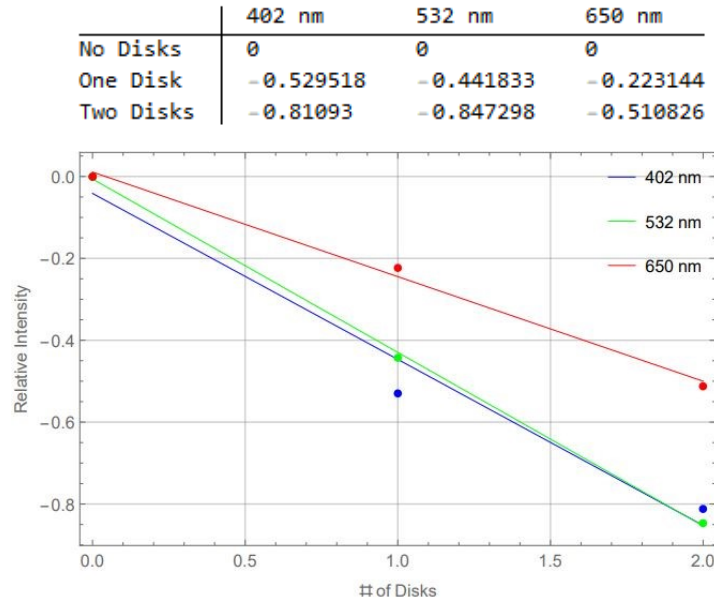


**Figure 3.9** Data points and corresponding linear fit to the natural log of the relative intensity of blue, green, and red wavelengths through 2 mm gadolinium acrylic disks

by the material's response to different wavelengths. Thus, we determined, it would be useful to calculate  $a$  to better characterize the attenuation by taking the natural logarithm of the data and then finding the resulting line's slope. Table 3.1 presents our values for  $a$ , a dimensionless quantity, with respect to each wavelength. Here you can see that the attenuation appears to be highest for the blue wavelength. These wavelengths constitute only a fraction of the possible wavelengths of electromagnetic waves preventing any extrapolation, but these values do show that the detector will absorb a significant amount of the blue light from the liquid scintillator.

From our theoretical calculations of the transmittance through three acrylic disks at 402 nm, only 28% of the total optical signal would be transmitted. However, experimentally, approximately 36% of the optical signal was transmitted through three acrylic disks and 50% through two disks. The discrepancy between these values could be due to the fact that our wavelength was not exactly 402 nm. The laser specifications gave a wide possible range for the wavelength going as low as

**Table 3.2** A list of the calculated attenuation coefficients for the given wavelength  $\lambda$  in 2 mm gadolinium acrylic disks

$\lambda$ (nm)	Attenuation Coefficient
402	0.40547
532	0.42365
650	0.25541

390 nm. Thus, at this wavelength, more light could have been transmitted. Practically, we are more concerned with how much light is actually transmitted through acrylic so for the purposes of calculation, we used the signal attenuation determined from our experiment outlined in Chapter 2.

When the attenuation experiment was again performed, the results, as shown in Fig. 3.9, were slightly different from the results using plain acrylic disks. The attenuation for 650 nm light remained fairly consistent, but the 532 nm light and 402 nm light both showed greater attenuation than the previous experiment. Specifically, for the 402 nm laser, as calculated using the value of  $a$  from Table 3.2, approximately 44% of the light was transmitted through two disks.

### 3.3 Conclusion

Our optical experiments, though not actual detector data, indicate that a detector constructed with this geometry and similar materials would be capable of collecting accurate data should the detector be constructed. From our comparison with Fresnel coefficients, once the gadolinium-acrylic disks are submerged in liquid scintillator, reflections from the scintillator-acrylic interface will be significantly less than at the air-acrylic interfaces due to the decrease in the reflectivity. When this attenuation from the acrylic disks is combined with nearly 85% transmission in the mineral oil, shown in Fig. 3.10, the total attenuation, the product of those two values, leads to approximately 61.2% attenuation for an optical signal traveling through the entire detector. For the minimum

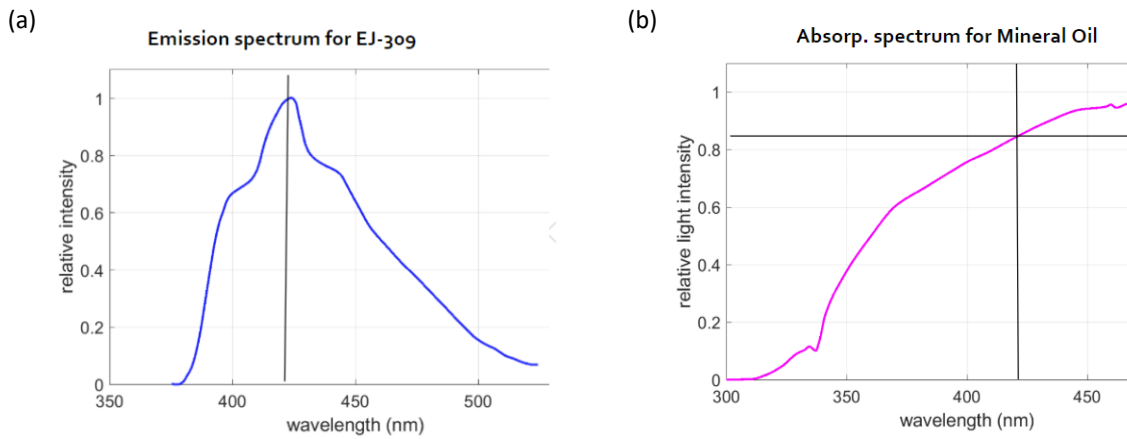


**Figure 3.10** These plots compare the emission spectrum of mineral-oil-based scintillator EJ-309 and an absorption spectrum for mineral oil with a point shown corresponding to the peak emission wavelength from EJ-309.

photon energies from proton recoil interactions for 0.5 MeV incident neutrons, found in the MCNP simulations, this attenuation leads to signals around 18.6 keVee, which is lower than our established standard of 100 keVee. However, for every other energy of incident neutron, both proton recoil and neutron capture events produce photons which are greater than 100 keVee after attenuation. In reality, a mineral-oil-based scintillator would produce photons throughout the entire body of the detector so the effective attenuation would actually be less than the 61.2% estimated earlier, but that value serves a purpose as an effective minimum value.

When we consider that the minimum photon energy for neutron capture in gadolinium is around 1 MeVee and large proportion of photons with energies up to around 4 MeVee, even around 70% attenuation would yield an optical signal with energy over 100 keVee. We can conclude that a detector with this geometry will maintain optical signal strength over 100 keVee even in the presence of signal attenuation. With the gadolinium isopropoxide disks, the actual attenuation factor was 62.6%, which is greater than the plain acrylic disks but, as explained previously, can still maintain an optical signal strength over 100 keVee.

## **3.4 Suggestions for Further Work**

Given the optical results presented, our next step in research is to construct the neutron detector according to our previously stated design. Using this detector, we would determine its neutron detection efficiency and ability to discriminate those events from gamma radiation. These qualities could then be used to determine if this our detector would be a viable replacement for existing neutron detectors.



# Bibliography

- [1] W. N. Association, “World Nuclear Performance Report 2018,” World Nuclear Performance Report (August 2018).
- [2] G. F. Knoll, *Radiation detection and measurement*, 3rd ed. ed. (John Wiley Sons, New York, 2000).
- [3] G. L. Jensen, D. R. Dixon, K. Bruening, and J. Bart Czirr, “A moderating  $^6\text{Li}$ -glass neutron detector,” *Nuclear Instruments and Methods In Physics Research* **220**, 406–408 (1984), cited By :2.
- [4] S. C. Howell, “LITHIUM GADOLINIUM BORATE CRYSTAL SCINTILLATOR FOR LOW FLUX NEUTRON DETECTION,” Senior Thesis (Brigham Young University, Provo, U.T.,2009).
- [5] N. Mena, M. Villani, S. Croft, R. B. McElroy, S. A. Philips, and J. B. Czirr, “Evaluation of lithium gadolinium borate capture-gated spectrometer neutron efficiencies,” *IEEE Transactions on Nuclear Science* **56**, 911–914 (2009), cited By :10.
- [6] A. McClellan, “Hybrid Liquid Organic Scintillator and Lithium-6 Neutron Detector: Correlated Pulses,” Senior Thesis (Brigham Young University, Provo, U.T.,2016).



# Index

Attenuation, 18, 20

Gamma discrimination, 2, 3

Neutron capture, 4, 6, 11, 13, 14, 20, 21

neutron capture, 4

Neutron capture efficiency, 2

Photomultiplier tubes, 4, 11, 12

Proton recoil, 4, 14, 22

Scintillator, 2–6, 28, 29

Transmittance, 10, 19